Essential Readings in Light Metals: Electrode Technology for Aluminum Production.
Edited by Alan Tomsett and John Johnson.

Light Metals — From ***Light Metals 1996***, Wayne Hale, Editor

TIN DIOXIDE-BASED CERAMICS AS INERT ANODES FOR ALUMINIUM SMELTING: A LABORATORY STUDY

A.M. Vecchio-Sadus, D.C. Constable, R. Dorin and E.J. Frazer
CSIRO Division of Minerals, PO Box 124, Port Melbourne, Victoria 3207, Australia

I. Fernandez, G.S. Neal, S. Lathabai and M.B. Trigg
CSIRO Division of Materials Science and Technology, Locked Bag 33, Clayton, Victoria 3168, Australia

Abstract

The behaviour of tin dioxide-based ceramics as inert anodes was examined in a laboratory-scale aluminium smelting cell over a range of electrolyte compositions with operating temperatures between 830 - 975°C. Anodes of a nominal composition SnO_2 (96 wt%), Sb_2O_3 (2 wt%) and CuO (2 wt%), were electrolyzed for 90 min at a current density of ~1 A cm^{-2}. The corrosion rate was determined from the tin and copper concentrations in the recovered electrolyte, aluminium metal and the fume. The corrosion rates were 12.5, 1.6 and 6.5 mg $(Ah)^{-1}$ in electrolytes with bath ratios 1.5 (975°C), 0.89 (903°C) and 0.74 (830°C), respectively. A four-fold increase in corrosion rate was obtained at open-circuit demonstrating the protection provided by oxygen evolution during electrolysis. A preliminary investigation of the dependence of corrosion rate on firing temperatures and additive (Sb_2O_3 and CuO) concentrations was conducted using a part-factorial design experiment. Post-electrolysis examination of the anodes using scanning electron microscopy coupled with energy dispersive spectroscopy analysis revealed a depletion of copper from the anode and a build-up of an alumina-rich surface layer under certain conditions.

Introduction

Substantial efforts have been directed towards the development of non-consumable ("inert") anodes for the aluminium smelting industry, but while a vast array of materials has been patented for use as inert anodes, none are in commercial use. The field has been surveyed extensively [e.g., 1-4] and recent research on ceramic oxides, cermets and metal alloys has been reviewed by Pawlek [5].

A primary criterion for an inert anode material is that it must be relatively insoluble in the cryolite-based electrolyte, yet the various materials tested exhibit a degree of solubility which may result in contamination of the aluminium product. The most promising materials which meet this criterion are the electronically conducting oxides with very low solubilities, of which tin dioxide-based ceramics have been identified as likely candidates [1]. Tin dioxide-based inert anodes were developed by Alusuisse [6] in 1976 and further investigated by Conradty [7]. The most systematic evaluation of their performance was carried out by Xiao et al. [8,9] who reported the effect of alumina concentration, bath ratio and current density on corrosion rate.

This paper reports the fabrication and performance of tin dioxide-based ceramics as candidate inert anodes for aluminium smelting. Studies were conducted in a laboratory-scale cell in several electrolyte compositions. In addition to corrosion and electrochemical behaviour, other cell operating characteristics such as current efficiency, anode bubble behaviour and anode potential were also examined. A preliminary investigation of the dependence of corrosion rate on additive (Sb_2O_3 and CuO) concentrations was conducted using a part-factorial design experiment. Post-electrolysis characterization of the anode materials was carried out by scanning electron microscopy and energy dispersive spectroscopy.

Experimental

Anode fabrication

Standard anodes. Tin dioxide-based anodes with a nominal composition SnO_2 (96 wt%), Sb_2O_3 (2 wt%) and CuO (2 wt%) were prepared using analytical reagent grade powders (Aldrich, 99.9%). Powders were placed in polyethylene jars with isopropanol, and milled using TZP (tetragonal zirconia polycrystalline phase) milling media (diam. 10 mm) for 18 h. The milled powder slurry was dried at 80°C for 24 h, screened to -500 μm and stored in air until required. Samples (120 g) were pressed uniaxially at 14 kPa in a hardened steel die (diam. 38 mm). The green bodies were fired in air at 200°C h^{-1} to 1290°C, held for 8 h, then cooled at 200°C h^{-1} to ambient temperature. The fired electrodes with densities of ~ 6.6 g cm^{-3}, were ground to size (diam. 25 mm × 50-75 mm long) with a 5° convex taper on the working face and leaving a 10 mm diameter stub for electrical connection. The anodes were cemented with calcium aluminate into high purity recrystallized alumina tubes with only the tapered face exposed to define the surface area (~5 cm^2). They were heated at 200°C h^{-1} to 1100°C, with a 2 h dwell to set the cement.

Part-factorial design anodes. Tin dioxide-based anodes with varying concentrations of Sb_2O_3 and CuO were prepared according to the compositions in Table I.

Furnace and electrochemical cell design

A detailed description of the multi-element electrochemical cell and furnace has been given elsewhere [10-12]. Electrolyses were performed in an atmosphere of argon in order to minimize oxidation of the graphite cell components and the furnace tube. The cell was equilibrated for one hour after the furnace had attained its working temperature. The electrolyte temperature was measured with a Type-K chromel-alumel thermocouple.

The anode stub was attached via a collet to the Inconel rod (see Figure 1). A molybdenum cathode (Metallwerk Plansee GmbH, 99.95%; diam. 24.9 mm) allowed the recovery of the aluminium product for direct current efficiency calculation. It had a complementary conical cross-section with a 170° included angle; the inter-electrode distance was a nominal 3 cm. An aluminium/cryolite reference electrode of the

"wetted molybdenum hook" design described by Burgman et al. [13] was used, and filled with the same electrolyte composition as the bulk.

Table I Composition of Part-Factorial Design Anodes

Anode Code	Firing Temp. (°C)	$[SnO_2]$ (wt%)	$[Sb_2O_3]$ (wt%)	[CuO] (wt%)	Fired density (g cm^{-3})
SED1	1302	98.33	1.31	0.36	6.36
SED2	1338	98.33	1.31	0.36	6.14
SED3	1302	95.95	3.69	0.36	3.05
SED4	1338	95.95	3.69	0.36	3.53
SED5	1302	97.68	1.31	1.01	5.92
SED6	1338	97.68	1.31	1.01	6.34
SED7	1302	95.30	3.69	1.01	6.39
SED8	1338	95.30	3.69	1.01	6.30
SED9	1320	96.82	2.50	0.68	6.36
SED10	1320	96.82	2.50	0.68	6.28
SED11	1290	96.82	2.50	0.68	6.43
SED12	1350	96.82	2.50	0.68	6.22
SED13	1320	96.82	0.50	0.68	5.62
SED14	1320	94.82	4.50	0.68	4.81
SED15	1320	97.36	2.50	0.14	2.43
SED16	1320	96.27	2.50	1.22	6.19
SED17	1320	96.82	2.50	0.68	6.32
Standard	1290	96.00	2.00	2.00	6.60

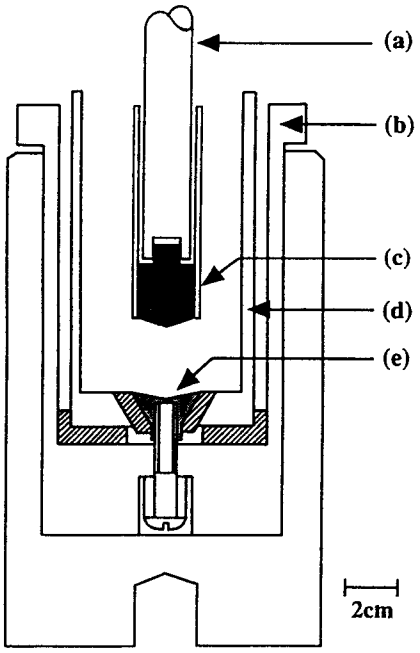

Figure 1: Schematic of multi-element graphite cell: (a) Inconel rod and collet, (b) outer graphite sheath (c) inert anode and alumina sheath (d) inner graphite sheath, (e) molybdenum cathode.

Electrolyte composition

The electrolyte (300 g) was composed of vacuum-dried synthetic cryolite (Onoda Chemical Industry Co. Ltd), alumina (ex. Comalco), aluminium fluoride (CERAC Inc., 99.9%), calcium fluoride (Aldrich, 99.9%), lithium fluoride (Aldrich, 99.9%) and magnesium fluoride (Aldrich, 99.9%) mixed according to the compositions in Table II. Alumina concentrations at saturation were employed to allow cell operation for reasonable periods and to minimize attack on the alumina sheath around the anode. Excess alumina (equivalent to 4 wt%) was added to maintain saturation during electrolysis for extended periods. Electrolyses were run at a constant superheat of 10°C.

Table II Electrolyte Compositions and Operating Temperatures

	Na_3AlF_6 (wt %)	Al_2O_3 (wt %)	AlF_3 (wt %)	CaF_2 (wt %)	LiF (wt %)	MgF_2 (wt %)	BR	$T_{oper.}$ (°C)
I	90.0	10.0	-	-	-	-	1.50	975
II	69.8	6.0	19.2	5.0	-	-	0.89	903
III	51.8	5.0	24.7	4.0	5.0	0.5	0.74	830

BR: defined as wt NaF/ wt AlF_3

Evaluation of anode performance

Open-circuit corrosion. The open-circuit corrosion of anode materials was determined by simple immersion tests. Anodes were suspended in the electrolyte for fixed periods and then removed into the cool zone of the furnace tube.

Electrolysis. A positive potential was applied to the candidate anode prior to immersion; the anode was then gradually lowered into the electrolyte over a period of 10 min until it had reached the operating inter-electrode distance. The electrolysis was conducted at a nominal current density of ~ 1 A cm^{-2} for ~27 000 Coulombs (5 A, ~ 90 min) using a scanning potentiostat (EG&G Princeton Applied Research, Model 362) coupled to a current booster (EG&G Princeton Applied Research, Model 365). Several experiments were conducted for extended periods (up to 72 000 Coulombs). Polarization curves were taken towards the end of the experiment by ramping the current down at 10 mA s^{-1} from 5 A to zero and recording the response on a Hewlett Packard X-Y recorder (Model 7045B). The anode-reference potential and resistance (measured as described in [12]) were sampled digitally (see below) to allow the later application of iR correction. A "junction potential" between the cathode aluminium pool and the reference electrode was measured at the end of the electrolysis and used to correct potential data.

At the termination of the electrolysis, the anode was removed to the cool zone of the furnace and the electrolyte allowed to solidify. The electrolyte, aluminium metal and the fume (condensed in the upper zone of the furnace tube) were collected for analysis. Current efficiencies were determined from the weight of the aluminium product using Faraday's law. The weight of aluminium was corrected for the molybdenum dissolved from the cathode substrate (up to 10 wt% at 975°C); no correction for the co-deposition of sodium (usually < 0.7 wt %) was made.

The anode-reference potential and resistance were monitored continuously on a Yokogawa HR1300 hybrid recorder. Periodically, they were sampled digitally for 40 s at 100 Hz using a Keithley Metrabyte DAS-HRES 16 bit multi-channel A/D interface board in an IBM-PC/AT compatible computer driven by software routines written in QuickBASIC (Microsoft Corporation). The stored data were analysed later and displayed using DADiSP 3.00B (DSP Development

Corporation) software to obtain anode bubble characteristics such as size and frequency.

Analytical methods

The tin, copper and antimony concentrations in the recovered electrolyte, aluminium metal, and the fume were determined by ICP. The whole aluminium disc and collected fume were submitted for analysis. As a grab sample of the electrolyte composition was found to be non-representative of the bulk, the entire electrolyte was hammer-milled to -100 mesh and riffled down to two 0.5 g samples for analysis. These samples were then fused with 12-22 flux (35.3 wt% $Li_2B_4O_7$, 64.7 wt% $LiBO_2$) and 0.5 cm^3 of 10% $LiNO_3$ solution and made up to 100 cm^3 for analysis.

Results and Discussion

Operating conditions

The finite solubility of tin dioxide in cryolite-based electrolytes has several implications for the operation of aluminium smelting cells. Solubilities of 0.08 wt% and 0.01 wt% have been reported in pure cryolite [15] and in cryolite/5 wt% alumina [16], respectively. In order to minimize anode solubility, the electrolyte should have a relatively high alumina concentration and the cell should be operated at low temperatures [8,14]. Thus, all the experiments reported here were conducted in alumina saturated electrolytes.

Evaluation of standard anodes at open-circuit

Experiments at open-circuit showed that significant corrosion (measured as total mass loss of SnO_2 and CuO) occurred within 15 min of immersion (Figure 2). Electrolyte composition I appeared to be more corrosive than composition II and this may be attributed to the higher operating temperature (i.e., 975°). The amount of corrosion for electrolyte composition I at ~110 min was three times greater than for composition II.

Corrosion (in mg) at open-circuit appeared to be more extensive than during electrolysis, there being a four-fold increase within the same time period compared with that obtained under electrolysis (see following section). It is likely that the active surface of the anode is more resistant to attack by the electrolyte when it is polarized as a result of the protective influences, both physical and chemical, of the layer of oxygen bubbles evolving on the anode surface. For this reason, all anodes to be electrolyzed were immersed into the molten electrolyte under an applied positive potential.

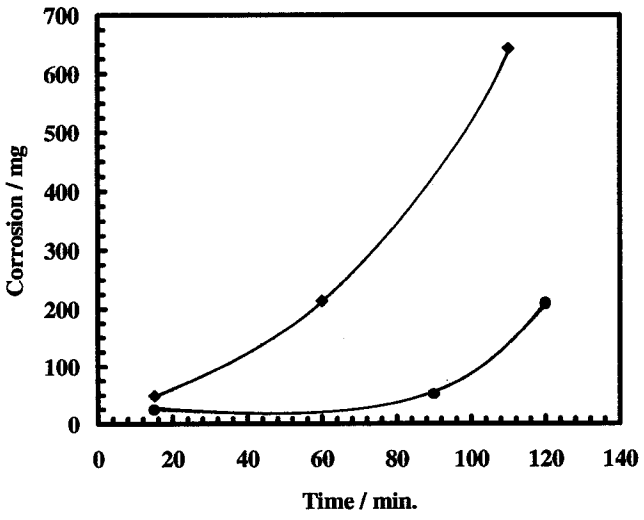

Figure 2: Change in the open-circuit corrosion with time in electrolyte compositions I (◆) and II (●).

The corrosion rates for electrolyte compositions I (BR 1.50) and II (BR 0.89) correspond to 70.2 and 20.9 mg cm^{-2} h^{-1}, respectively. A comparable experiment by Yang et al. [17,18] in a BR 1.4 electrolyte gave a corrosion rate of 0.918 mg cm^{-2} h^{-1}; this value may be low because it is based on the measurement of very small changes in anode volume and mass.

Evaluation of standard anodes under electrolysis

The corrosion rate was calculated from the total mass of the tin and copper (expressed as the oxides) in the recovered electrolyte, aluminium metal and the fume (Table III). Antimony levels were extremely low, reflecting the apparent loss of this material during the sintering of the anode. An examination of the data (Table IV) showed that up to 98% of the corrosion products were found in the electrolyte.

Table III Average Tin and Copper Content (wt%) in Various Components After Testing Standard Tin Dioxide-Based Anodes

Electrolyte	Electrolyte		Metal		Fume	
Composition	Sn	Cu	Sn	Cu	Sn	Cu
I	0.016	0.005	0.130	0.012	0.573	0.0005
II	0.001	0.002	0.005	0.002	0.069	0.034
III	0.011	0.002	0.013	0.0001	0.018	0.036

Table IV Distributions of the Corrosion Products After Testing With Standard Tin Dioxide-Based Anodes

Electrolyte Composition	% Electrolyte	% Metal	% Fume	CuO/SnO_2 (wt / wt)
I	93.2	3.7	3.1	0.24
II	88.1	1.8	10.1	1.63
III	97.8	0.8	1.4	0.18

Effect of electrolyte composition. The effect of electrolyte composition on corrosion rate is shown in Table V. (Because of the choice of current (5 A) and anode area (~5 cm^2), the corrosion rate when quoted in mg $(Ah)^{-1}$ is equivalent to mg cm^{-2} h^{-1}.) The best performance of tin-dioxide based anodes occurred in an alumina-saturated electrolyte with BR 0.89 operating at 903°C. An anticipated improvement in corrosion rate with decreasing temperature was not

Table V Performance Summary of Standard Tin Dioxide-Based Anodes

Electrolyte Composition	Number of Samples	Current Efficiency (%)	Corrosion Rate ± s.d. ~27 000 Coulombs mg $(Ah)^{-1}$
I	9	85-90	12.5 ± 2.3
II	7	98-100	1.6 ± 0.2
III	8	91-97	6.5 ± 0.9

achieved in electrolyte composition III containing LiF (to increase the electrolyte conductivity). Instead, a four-fold increase in corrosion rate was obtained. Wang and Thonstad [14] reported that high concentrations of LiF (> 5 wt%), and extremes of BR, had detrimental effects on the corrosion rate but the effect of increasing AlF_3 concentrations was less dramatic.

Effect of electrolysis time. A plot of corrosion rate versus charge passed is shown in Figure 3. The value at 27 000 Coulombs represents the mean of a large number of experiments, while the other points are averages of duplicate runs. Given the general shape of the plot, the point at 36 000 Coulombs would appear to be an outlier. Higher corrosion rates were obtained at shorter electrolysis periods, and a 'steady-state' level may be approached after ~30 000 Coulombs. This behaviour implies fast corrosion of the surface layer during the early stages of electrolysis and/or the build-up of a semi-protective layer (see, Characterization of anodes and corrosion mechanism).

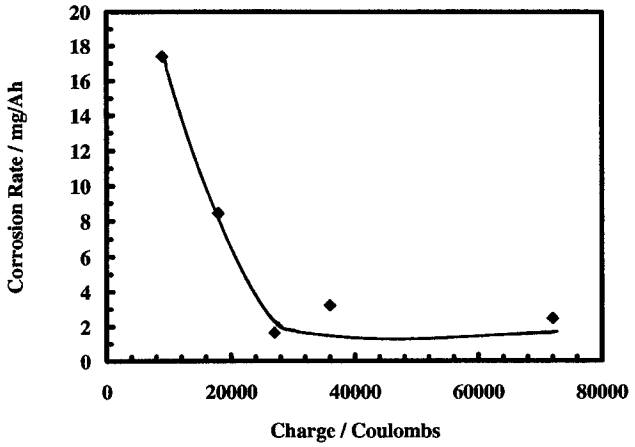

Figure 3: The dependence of corrosion rate upon charge in electrolyte composition II.

Current efficiency. Current efficiencies (see Table V) were comparable to those obtained with a graphite anode in the various electrolyte compositions [10] and no systematic variations were noted. Others [19] quoted current efficiencies of 88.96 compared with 87.20% for graphite, which they considered to be a statistically significant difference. The present results suggest that no detrimental effect on current efficiency can be expected when using an oxygen-evolving anode. This implies that the effect of oxygen evolution on the mass transfer rate to the cathode is not significantly different to carbon dioxide in this laboratory cell, and that the factor continuing to control the back reaction is the rate of transport of aluminium across the metal/electrolyte interface.

Polarization behaviour and operating voltages. Polarization curves for tin dioxide-based anodes in various electrolyte compositions are shown in Figure 4. These curves have been corrected for iR and the change in "junction potential" of the reference electrode in the different electrolytes.

As expected, there was an increase of approximately 1V for a cell operated with an inert anode versus a graphite anode (Table VI). As the BR was lowered, higher operating cell voltages were recorded and this trend is in accordance with the lower operating temperatures and the corresponding decrease in electrolyte conductivity. The difference in operating cell voltage between electrolyte compositions I and II is approximately 1 V, and between I and III approximately 1.5 V.

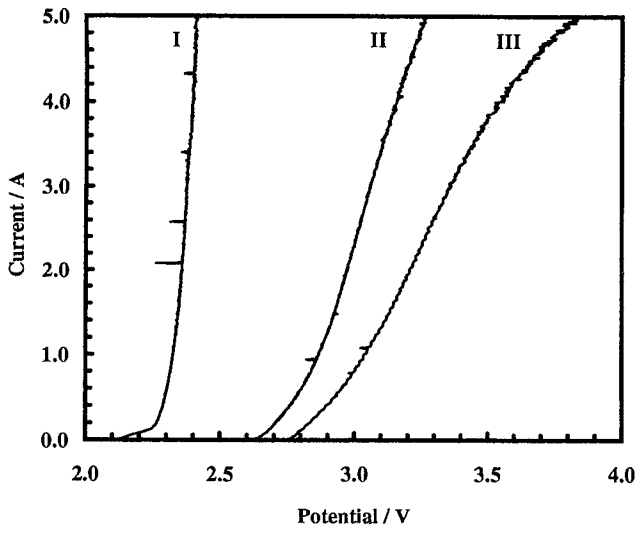

Figure 4: Representative polarization curves of tin dioxide-based anodes in electrolyte compositions I, II and III.

Table VI Operating Voltages for Standard Tin Dioxide-Based Anodes at a Current Density of 1 A cm^{-2}

Electrolyte Composition	Bath Ratio	Total Cell Voltage (V)	Polarization Voltage at 1 A cm^{-2} (V)
Tin dioxide-based anodes			
I	1.50	3.75	0.28
II	0.89	4.69	0.64
III	0.74	5.21	1.11
Graphite			
I	1.5	2.88	~0.5 [22]

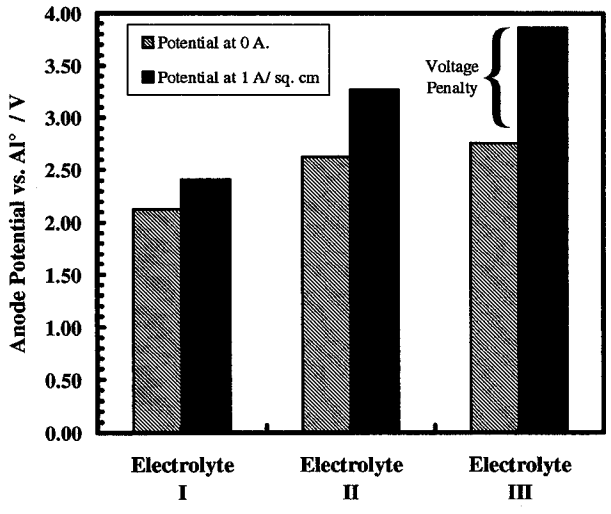

Figure 5: Comparison of open-circuit and operating potentials for tin dioxide-based anodes in various electrolytes.

An analysis of anode potentials corrected for iR drop and the "junction potential" of the reference electrode is shown in Figure 5. This figure shows that there is an increase of ~ 0.6 V in the open-circuit anode potential between electrodes operated in electrolyte I, and in electrolytes II and III. Furthermore, although the overpotential at 1 A cm^{-2} in electrolyte I is only 0.28 V, significant increases in this overpotential are seen in electrolytes II (0.64 V) and III (1.1 V). This compares with 0.1-0.2 V for electrolysis at a current density of 0.6-1.0 A cm^{-2} in BR 1.35 reported by other workers [14,20,21].

Electrochemical impedance spectroscopy (EIS). A series of electrochemical impedance spectra were taken of a standard tin dioxide-based anode at open-circuit following 15 minute intervals of electrolysis at 1 A cm^{-2} in electrolyte II. The equipment used was a Schlumberger Electrochemical Interface (Model SI 1286) coupled to a Schlumberger Frequency Response Analyser (Model SI 1155) and driven from a 486DX IBM-compatible computer using "ZPlot/ZView for Windows V.1.1D" software (Scribner Associates Inc.).

Windish Jr. [23] reported the interference of gas bubbling during EIS measurements of cermet anodes. To avoid this interference, the anode was allowed to stand at open-circuit for two minutes prior to taking the impedance spectrum. This allowed the gas bubbles to disperse and the stabilization of conditions at the electrolyte/anode interface.

The spectra in the Nyquist diagrams in Figure 6, show the progressive development with electrolysis time of a linear (Warburg) response in the low frequency region of the impedance plot. This behaviour can be explained in terms of the anode pores being gradually filled by the electrolyte thus allowing the electrolysis to occur deeper into the anode surface layer. This interpretation is supported by the observed penetration of electrolyte species into the anode surface microstructure (see section, Characterization of anodes and corrosion mechanism). The predominance of the linear portion of this plot, over the almost non-existent semi-circular section [23] at the high frequency end, is an indication that the corrosion reaction is primarily diffusion controlled.

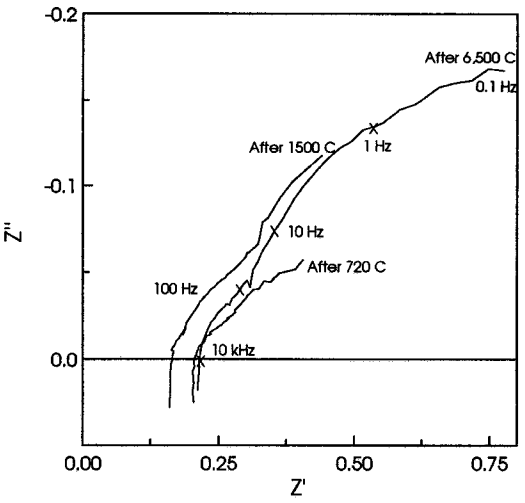

Figure 6: Complex plane plots for a standard tin dioxide-based anode taken at open-circuit following electrolysis for various times. Frequencies shown (marked as ×) are for the 6500 Coulombs plot.

Bubble evolution characteristics. The anode-reference potential and resistance were sampled digitally to obtain bubble characteristics. In a previous communication [12], the mean bubble radius ($\langle r_d \rangle$) was calculated following the derivation of a proportionality constant (α_c = 0.86) for an inter-electrode distance of 3 cm. Since α_c is essentially a geometric shading factor, it is not expected to vary significantly with electrolyte composition.

Table VII shows the changes in bubble characteristics of tin dioxide-based anodes with electrolyte composition. In general, tin dioxide-based anodes showed smaller potential fluctuations than graphite anodes because of the formation of smaller bubbles. Similar behaviour has also been reported by other workers [19]. However, it should be noted that the graphite anodes were fitted with sleeves [10,11], which would tend to increase bubble size. As there is little difference in dominant bubble frequency (DBF) between the two types of anodes at longer electrolysis times (i.e., 60 min), one could expect a decrease in gas hold-up under the anode, a reduction in bubble layer thickness, and a corresponding small reduction in cell voltage for the tin dioxide-based anode.

Table VII Changes in Bubble Characteristics For Tin Dioxide-Based Anodes and Graphite Anodes with Electrolyte Composition

	Anode Type	$\langle r_d \rangle$ at 20 min (mm)	$\langle r_d \rangle$ at 60 min (mm)	DBF at 20 min (Hz)	DBF at 60 min (Hz)
I	tin dioxide	0.48	0.55	0.50	0.70
I	graphite[1]	0.73	0.64	0.65	0.50
II	tin dioxide	0.36	0.42	0.50	0.75
II	graphite[1]	0.91	0.73	0.90	0.70
III	tin dioxide	0.48	0.66	0.40	0.80
III	graphite[1]	0.64	0.49	0.80	0.80

[1] Using sleeved graphite anodes [11].

Evaluation of part-factorial design anodes

The raw materials, fabrication route and firing cycle can all affect the performance of an anode. The electrical conductivity [14,24,25] of the anodes is dependent upon the microstructure and, in particular, the presence of additives and secondary grain boundary phases. Sb_2O_3 increases the electrical conductivity of the ceramic and CuO assists in densification [26]. The standard composition of 96 wt% SnO_2, 2 wt% Sb_2O_3, 2 wt% CuO was selected for the above tests since it has excellent conductivity and has been used successfully in arc-furnace electrodes for the glass industry [25-28].

A preliminary investigation of the dependence of corrosion rate on firing temperatures and additive concentrations was conducted using a part-factorial design experiment. The independent variables were composition and firing temperature, and the dependent variables were fired density and corrosion rate. The Sb_2O_3 concentration was varied from 0.05 - 4.5 wt% (i.e., approximately half to double that of the standard composition) and the CuO concentration was varied from 0.14 - 1.0 wt% (i.e., approximately 0.07 - 0.5 that of the standard composition). The upper level of the CuO concentration was limited to half the level of the standard because of the preferential leaching of copper from the anode (see following section). All experiments were run in electrolyte composition II, as this composition, of the three electrolytes examined, gave the lowest corrosion rate for a standard tin dioxide-based anode. Table VIII shows the corrosion rates obtained in this study. Electrodes SED 3, 4, 5, 9, 14 and 15 did not densify (see Table I) and were either too fragile to mount or dislodged from the collet during the experiments; thus, their corrosion rates could not be determined.

Overall, the corrosion rates were in the range 1.2 - 5.7 mg $(Ah)^{-1}$. The lowest values were obtained for compositions SED 7 and SED 11, and are slightly lower than the value (1.6 mg $(Ah)^{-1}$) obtained for a standard composition tin dioxide-based anode. Because a significant number of the anodes could not be tested due to inadequate physical properties, there were insufficient data to allow a complete factor analysis and contour construction. Nonetheless, there are indications that lower corrosion rates may be obtainable by using lower firing temperatures.

Table VIII Corrosion Rates (mg $(Ah)^{-1}$) of Anodes for the Part-Factorial Design Experiment in Electrolyte Composition II

Code	Corrosion Rate	Firing Temp. (°C)	$[Sb_2O_3]$ (wt%)	[CuO] (wt%)
SED1	2.3	1302	1.31	0.36
SED2	5.7	1338	1.31	0.36
SED3	nd [1]	1302	3.69	0.36
SED4	nd [1]	1338	3.69	0.36
SED5	nd [1]	1302	1.31	1.01
SED6	2.2	1338	1.31	1.01
SED7	1.2	1302	3.69	1.01
SED8	3.3	1338	3.69	1.01
SED9	nd [1]	1320	2.50	0.68
SED10	2.5	1320	2.50	0.68
SED11	1.2	1290	2.50	0.68
SED12	5.6	1350	2.50	0.68
SED13	2.2	1320	0.50	0.68
SED14	nd [1]	1320	4.50	0.68
SED15	nd [1]	1320	2.50	0.14
SED16	1.6	1320	2.50	1.22
SED17	1.9	1320	2.50	0.68
Standard	1.6	1290	2.00	2.00

[1] Not determined due to physical properties.

Characterization of anodes and corrosion mechanism

A target performance (i.e., corrosion rate) for inert anodes has been suggested as 1-3 cm per year of service [14]. Recommendations to DOE [29] for inert anode retrofitting of conventional cells are based on an anode (nickel ferrite) lifetime of 5 years with a wear rate of 0.25 inches $year^{-1}$ (0.64 cm $year^{-1}$). The best corrosion rate of 1.6 mg $(Ah)^{-1}$ for a 5 cm^2 tin dioxide-based anode of standard composition (96 wt% SnO_2, 2 wt% Sb_2O_3, 2 wt% CuO) corresponds to a wear rate of ~2 cm per year.

Three corrosion mechanisms [24] for inert anodes have been identified: chemical dissolution (fluorination), reduction by dissolved metal, and disintegration [8,14]. Extensive corrosion can be caused by electrolytic decomposition of the anode material provoked by alumina depletion and can be accompanied by intergranular attack and disintegration (spalling). The aluminium reduction reaction apparently causes only a slight attack of the anode [18].

Evaluation of standard anodes. Microstructural examination (Leica Stereostand 360FE) of the as-fired tin dioxide-based anodes showed that the bulk of the material consisted of rounded grains of tin dioxide, ranging in size from 2-10 μm and exhibiting very clean grain boundaries. SEM also revealed small amounts of a second phase at some triple points. Energy dispersive spectroscopy (EDS) indicated that this phase contained copper, or copper and antimony.

The ratio of CuO to SnO_2 in the recovered electrolyte, aluminium metal and the fume was found to be significantly higher than the composition of the source anode (see Table IV). The ratios averaged 1:4, 1:0.6 and 1:5.7 for electrolyte compositions I, II and III, respectively, compared with 1:50 in the starting material. This result indicated a preferential "leaching" of copper from the anode which was confirmed by SEM. Microscopic examination of tested anodes also revealed a depletion of the copper-rich secondary phase to a depth of 50-100 μm but without significant disruption of the microstructure.

Although examination of the anodes after electrolysis revealed that the electrolyte had penetrated up to 700 μm into the anode, there was only about 100 μm penetration after standing at open-circuit for a comparable period of time. In this penetration zone, it appeared that much of the copper-rich second phase had leached out. The electrolyte composition had some influence on the post-electrolysis structure. Examination of anodes evaluated in electrolyte composition II showed that at some regions along the interface between the anode and electrolyte, a thin, alumina-rich layer had formed, which could be significant in limiting corrosion.

Evaluation of experimental design anodes. The microstructural examination of anodes from the part-factorial design conducted in electrolyte composition II showed no apparent differences in structure given the variations in the additive concentrations and firing temperature, even though the anodes were more porous than the standard composition. The amount of CuO-containing phases decreased as the CuO additive concentration was decreased. Except for the anode with the least amount of additive, the penetration of cryolite was <350 μm from the face of the anode. A thin, alumina-rich layer similar to that seen in the standard anodes, formed at the interface between the anode face and the frozen electrolyte.

Conclusions

The performance of tin dioxide-based anodes with a standard composition SnO_2 (96 wt%), Sb_2O_3 (2 wt%) and CuO (2 wt%) was evaluated in a laboratory-scale smelting cell. These materials operated as effective inert anodes in a range of electrolyte compositions (BR 1.5 - 0.74). A preliminary investigation of the dependence of corrosion rate on firing temperatures and additive concentrations was conducted using a part-factorial design experiment. The results of this study were inconclusive because a complete set of design points could not be obtained, but there were indications that decreasing the firing temperature would be beneficial.

The corrosion rates for standard tin dioxide-based anodes were 12.5, 1.6 and 6.5 mg $(Ah)^{-1}$ in electrolytes with bath ratios 1.5 (975°C), 0.89 (903°C) and 0.74 (830°C), respectively. The lowest corrosion rate of 1.6 mg $(Ah)^{-1}$ was obtained in electrolyte composition II and this corresponds to a wear rate of ~2 cm per year. This compares to recommendations for retrofitting inert anodes to existing cells of ~0.64 cm per year and thus, further optimization of the composition and fabrication is required. In addition, in this electrolyte, there was an increase in cell voltage due to decreased electrolyte conductivity and increased anodic overpotential. Such increases would need to be offset by advanced cell designs incorporating vertical bipolar electrodes.

Inert anode performance is improved by maintaining full anodic polarization and a coverage of oxygen. This was demonstrated by a four-fold increase in corrosion at open-circuit compared with the corresponding period under electrolysis. Post-electrolysis examination of anodes using scanning electron microscopy coupled with energy dispersive spectroscopy analysis revealed a depletion of copper from the anode and a build-up of an alumina-rich surface layer in a BR 0.89 electrolyte. This formation of this layer may be the major factor contributing to the relatively low corrosion rate in this electrolyte.

Acknowledgements

We thank J.F. Kubacki for cell construction and maintenance, R. Mann (University of Melbourne) for electrolyte sample preparation, P.M. Hoobin, C. McInnes and M. Anthony for analytical services, and Comalco and Alcoa for supply of some electrolyte materials.

References

1. H. Zhang, V. de Nora and J. A. Sekhar, Materials Used in the Hall-Heroult Cell for Aluminum Production, (USA: TMS, 1994) pp 15-35.

2. V. de Nora, "Non-Carbon Anodes for Aluminium Electrowinning", Dechema Monograph, **Vol. 125** (Germany: VCH, 1992), 377-387.

3. R.P. Pawlek, "Development of Anodes for Aluminium Elecrtolysis", Aluminium, **65** (1989) 1252 and 1258.

4. K. Billehaug and H. A. Øye, "Inert Anodes for Aluminium Electrolysis in Hall-Héroult Cells", Aluminium, **57** (1981) 146-150 and 228-231.

5. R.P. Pawlek, "Recent Developments of Inert Anodes for the Primary Aluminium Industry: Part I and II", Aluminium, **71** (1995) 202-206 and 340-342.

6. (i) H. Alder, (Swiss Aluminium Ltd): US Patent 3,960,678 (1976); US Patent 3,930,967 (1976); US Patent 3,974,046 (1976).

(ii) H.J. Klein, (Swiss Aluminium Ltd): US Patent 3,718,550 (1973).

7. C. Zollner and K. Kahl, "Dimensionsstabile Elektroden fur die Schmeltzfluss-elektrolyse", Report Conradty Nurenberg to Bundesministerium fur Forshung und Technologie, Bonn O1ZM012, (1985).

8. H. Xiao, R. Hovland, S. Rolseth and J. Thonstad, "On the Corrosion and the Behavior of Inert Anodes in Aluminum Electrolysis", Light Metals 1992, ed. E.R. Cutshall, (Warrendale, USA: The Minerals, Metals and Materials Society, 1991), 389-399.

9. H. Xiao, "On the Corrosion and the Behavior of Inert Anodes in Aluminium Electrolysis" (PhD thesis, Norwegian Institute of Technology, Trondheim Norway,1993).

10. A. M. Vecchio-Sadus, R. Dorin and E. J. Frazer, "Evaluation of Low-Temperature Cryolite-Based Electrolytes for Aluminium Smelting", J. Appl. Electrochem., **25** (1995) in press.

11. R. Dorin, E. J. Frazer and A. M. Vecchio-Sadus, "Current Efficiency, Mass Transfer & Bubble Evolution Characteristics in a Laboratory-Scale Alumina Reduction Cell with Optional Sleeved Anode", Light Metals 1994, ed. U. Mannweiler, (Warrendale, USA: The Minerals, Metals and Materials Society, 1993), 205-210.

12. R. Dorin and E. J. Frazer, "Operational Characteristics of Laboratory Scale Alumina Reduction Cells with Wettable Cathodes", J. Appl. Electrochem., **23** (1993) 933-942.

13. J. W. Burgman, J. A. Leistra and P. J. Sides, "Aluminum/Cryolite Reference Electrodes for Use in Cryolite-Based Melts", J. Electrochem. Soc., **133** (1986) 496-500.

14. H. Wang and J. Thonstad, "The Behavior of Inert Anodes as a Function of Some Operating Parameters", Light Metals 1989, ed. P.C. Campbell, (Warrendale, USA: The Minerals, Metals and Materials Society, 1988), 283-290.

15. H. Xiao, J. Thonstad and S. Rolseth, "A Study on the Solubility of SnO_2 in Cryolite-Based Melts", Molten Salt Forum, **1-2** (1993/94) 215-230.

16. A.I. Belyaev, M.B. Rapoport and L.A. Firsanova, Metallurgie des Aluminiums, (Berlin: VEB Verlag Chemie, 1956).

17. J. Yang, Y. Liu and H. Wang, "The Behavior and Improvement of SnO_2-Based Inert Anodes in Aluminium Electrolysis", Light Metals 1993, ed. S.K. Das, (Warrendale, USA: The Minerals, Metals and Materials Society, 1992), 493-495.

18. H. Wang, J. Yang, Y. Liu and J. Thonstad, "Corrosion Mechanism of SnO_2-Based Inert Anodes", Trans. Nonferrous Met. Soc. China, **2** (1992) 8-13, 20.

19. J. Thonstad and H. Xiao, "A Comparison of Current Efficiencies Obtained With Inert Anodes and Carbon Anodes in a Laboratory Aluminium Cell", Aluminium, **68** (1992) 1088-1090.

20. J. Thonstad, Y.X. Liu and S. Jarek, "Overvoltage on Inert Anode Materials in Cryolite Melts", Proc. 8th International Light Metals Meeting, Leoben-Vienna (1987) 150-154.

21. Y. Liu and H. Xiao, "Studies of the Anodic Process at SnO_2-Based Electrodes in Aluminium Electrolysis", Molten Salts, **Vol. 87-7** (USA: The Electrochemical Society, 1987) 751-752.

22. E.W. Dewing, "The Chemistry of the Alumina Reduction Cell", Can. Met. Quart., **30** (1991) 153-161.

23. C.F. Windisch Jr., "A Comparative EIS Study on Cermet and Platinum Anodes for the Electrolytic Production of Aluminum", Proc. Third International Symposium Electrochemistry in Mineral and Metal Processing III, **Proc. Vol. 92-17** (USA: The Electrochemical Society, 1992) 508-514.

24. Z. Yiu, J. Yang, H. Wang, Q. Zhao, Y. Liu and X. Gao, "Model of Conductivity in Doped SnO_2-Based Inert Anodes for Al-Electrowinning", Trans. Nonferrous Met. Soc. China, **2** (1992) 59-63.

25. I. Galasiu, R. Galasiu and I. Lingvay, "Tin Dioxide Based Semiconducting Ceramics as Inert Anodes", Acta Chim. Hungarica, **129** (1992) 557-563.

26. I. Galasiu and R. Galasiu, "Inert Anodes for Aluminium Electrowinning. I. Variation of Properties with Composition", VII Al Symposium, Slovakia (1993) 57-68; "Inert Anodes for Aluminium Electrowinning. II. Variation of Properties with the Preparation Method", VII Al Symposium, Slovakia (1993) 69-75.

27. M. Zaharescu, S. Mihai, S. Zuca and K. Matiasovsky, "Contribution to the Study of SnO_2-Based Ceramics. Part I. High-Temperature Interactions of Tin(IV) Oxide With Antimony(III) Oxide and Copper(II) Oxide", J. Materials Sci., **26** (1991) 1666-1672.

28. M. Zaharescu, M. Terzi, S. Zuca and K. Matiasovsky, "Contribution to the Study of SnO_2-Based Ceramics. Part II. Effect of Various Oxide Additives on the Sintering Capacity and Electrical Conductivity of SnO_2", J. Materials Sci., **26** (1991) 1673-1676.

29. J.W. Galambas, G.L. Eitel and J.R. Payne, "Cost Effectiveness Study For Retrofitting American Aluminum Production Plants With Inert Anode-Cathode Systems", Stone & Webster Engineering Corporation, DOE/RL-88-25 (USA: Washington, Nov. 1988).